crystals

MDPI

Article

An Environmentally Friendly Method for Removing Hg(II), Pb(II), Cd(II) and Sn(II) Heavy Metals from Wastewater Using Novel Metal–Carbon-Based Composites

Abdel Majid Adam [1,*], Hosam A. Saad [1], Ahmed A. Atta [2], Mohammed Alsawat [1], Mohamed S. Hegab [3], Tariq A. Altalhi [1] and Moamen S. Refat [1]

[1] Department of Chemistry, College of Science, Taif University, P.O. Box 11099, Taif 21944, Saudi Arabia; HAS@tu.edu.sa (H.A.S.); Mohammed@tu.edu.sa (M.A.); TariqAltalhi@tu.edu.sa (T.A.A.); msrefat@tu.edu.sa (M.S.R.)
[2] Department of Physics, College of Science, Taif University, P.O. Box 11099, Taif 21944, Saudi Arabia; AAA@tu.edu.sa
[3] Deanship of Supportive Studies, Taif University, P.O. Box 11099, Taif 21944, Saudi Arabia; MSH@tu.edu.sa
* Correspondence: majidadam@tu.edu.sa

Abstract: Rapid economic and industrial development and population growth have made water contamination a serious environmental problem and a major threat to public health worldwide. Heavy metals are extensively used in numerous industrial applications and are some of the most important environmental contaminants. The impacts of heavy metals on the health of humans, animals, and plants make their removal from wastewater and water resources an important and vital issue. In this study, a simple and environmentally friendly method is proposed for the synthesis of a $ZnFe_2O_4$-carbon nanotube (CNT) adsorbent material. SEM/EDX analysis and Fourier-transform infrared spectrophotometry (FTIR) are used to characterize the synthesized adsorbent material. We test the synthesized adsorbent material's ability to recover four heavy metals (Hg(II), Pb(II), Cd(II) and Sn(II) ions) from an aqueous solution. We show that crushing fullerene CNTs with the $ZnFe_2O_4$ composite improves the adsorption properties of free fullerene CNTs towards the investigated heavy metal ions by 25%.

Keywords: carbon nanotubes; metal oxide composite; heavy metals; environmental remediation; nanomaterials and applications

Citation: Adam, A.M.; Saad, H.A.; Atta, A.A.; Alsawat, M.; Hegab, M.S.; Altalhi, T.A.; Refat, M.S. An Environmentally Friendly Method for Removing Hg(II), Pb(II), Cd(II) and Sn(II) Heavy Metals from Wastewater Using Novel Metal–Carbon-Based Composites. *Crystals* **2021**, *11*, 882. https://doi.org/10.3390/cryst11080882

Academic Editors: Claudia Graiff and Zhaohui Li

Received: 1 July 2021
Accepted: 26 July 2021
Published: 29 July 2021

1. Introduction

Water is critical for sustaining life on planet earth, as water covers around 71% of the total surface area. Unfortunately, only 1% of the total water is suitable for drinking [1]. A significant amount of environmental water pollution has been caused by the rapid progress and development of industrial technology, the fast growth of human society, and the increasing global population. Freshwater resources are still limited and the demand for freshwater is increasing yearly. Water contaminants include dyes, organics, viruses, bacteria, and heavy metal ions, such as mercury, chromium, arsenic, nickel, zinc, cadmium, and lead, with their non-biodegradable nature posing a great risk to human health. Water pollution from heavy metals is threatening the environment. Rapid industrial development has led to an increase in the contamination of water resources by heavy metals due to the discharge of their industrial wastewater. The effluents discharged from several industries to the hydrosphere contain higher levels of heavy metals, which are carcinogenic, mutagenic, toxic, and pose a significant source of pollution due to their recalcitrant nature. They can cause many adverse effects such as nephritic syndrome, encephalopathy, anemia, miscarriages, hepatitis, kidney damage, and cancer. Heavy metals are harmful to humans, animals, and plants due to their propensity to bioaccumulation, as well as their high toxicity and carcinogenicity. Mercury (Hg), lead (Pb), cadmium (Cd), tin (Sn), arsenic (As), and

other heavy metals are extremely toxic to humans, even at very low concentrations of several micrograms per liter [2–6]. Working out how to eliminate these contaminations from water resources and wastewater has become an urgent problem. This problem challenges researchers and industrialists around the globe to develop innovative routes to remove these hazards. The two general categories of treatment approaches for the recovery of heavy metal from water or wastewater are as follows [7]: chemical methods, such as oxidative processes, chemical precipitation, chemical degradation, chemical reduction, and photochemical and electrochemical destruction; physical methods, such as membrane filtration, membrane separation, adsorption, ion exchange, sorption techniques, flotation, ion exchange, coagulation, electrocoagulation, irradiation, and flocculation.

Among these approaches, adsorption techniques to eliminate heavy metals from aqueous media have become more attractive, have received worldwide attention, and are considered to be some of the most promising techniques due to their powerful performance, low energetic requirements, ease of implementation and operation, safety, and low cost [8–10]. Several adsorbents, including metal oxides, resin, silicate materials, clays, polymers, polymer–metal oxide hybrids, biomaterials, and nanocomposites, as well as carbonaceous materials, including activated carbon, carbon–graphene-based materials, fullerenes, and biochar, are newly developed and display potential applications in the removal of heavy metals from water or wastewater [11–23]. Fullerenes have a hydrophobic character, high electron affinity, a high surface-to-volume ratio, and surface defects. Fullerenes have numerous applications, including in semiconductors, electronics, biomedical sciences, solar cells, sensors, cosmetics, artificial photosynthesis, and surface coatings [24,25]. The defects, lower aggregation tendency, and large surface area make fullerenes useful materials for the recovery of pollution from wastewater.

Ferrites or ferrimagnetic oxides are extremely attractive materials due to their high applicability in nanotechnology and outstanding physical properties. Spinel-type transition metal ferrites (MFe_2O_4; M–Mg, Mn, Co, Ni, Zn, etc.) are a group of important magnetic materials that are widely used in many fields, such as cancer therapy, drug delivery systems, electronic devices, catalysts, adsorbents for the removal of heavy metal ions, and magnetic recording media. Zinc ferrite ($ZnFe_2O_4$) is an n-type semiconductor, having a spinel structure and narrow band gap (1.86 eV). Several techniques have been used to synthesize $ZnFe_2O_4$, such as electrodeposition, sol–gel, hydrothermal, co-precipitation, and microemulsion techniques [26–32]. Our aim in this investigation is to improve the adsorption properties of fullerene CNT towards organic dyes by combining the fullerene CNT with the $ZnFe_2O_4$ composite. This study involves three steps: (i) synthesizing a $ZnFe_2O_4$ composite from the co-precipitation of urea and iron(III) chloride with a zinc salt ($ZnCl_2$ or $Zn(CH_3COO)_2{\cdot}2H_2O$)]; (ii) synthesizing an adsorbent material by crushing the resultant $ZnFe_2O_4$ composite with fullerene carbon nanotube (CNT); (iii) examining the adsorption performance of the synthesized adsorbent material towards the removal of several heavy metal ions (i.e., Hg(II), Pb(II), Cd(II), and Sn(II)) from aqueous solution.

2. Reagents, Material Characterization and Methods

2.1. Reagents

Alfa Aesar (Thermo Fisher Scientific, Kandel, Germany) provided the multiwalled fullerene carbon nanotubes (CNTs) (95% nanotubes, 0.1–10 micron long, 1–3 nm ID, 3–20 nm OD). Sigma-Aldrich (Saint Louis, MO, USA) provided the metal salts used in this investigation, namely zinc chloride ($ZnCl_2$; 136.30 g/mol; purity $\geq$ 98%), zinc acetate ($Zn(CH_3COO)_2{\cdot}2H_2O$; 219.51 g/mol; purity $\geq$ 98%), iron (III) chloride ($FeCl_3$, 162.20 g/mol, purity $\geq$ 99.99%), mercury(II) nitrate monohydrate ($Hg(NO_3)_2{\cdot}H_2O$; 342.62 g/mol; purity $\geq$ 98.5%), lead (II) acetate trihydrate ($Pb(CH_3COO)_2{\cdot}3H_2O$; 379.33 g/mol; purity $\geq$ 99.99%), cadmium nitrate tetrahydrate ($Cd(NO_3)_2{\cdot}4H_2O$; 308.48 g/mol; purity $\geq$ 99.0%), and tin (II) chloride ($SnCl_2$; 189.62 g/mol; purity $\geq$ 99.99%). Urea (NH_2CONH_2; 60 g/mol; purity $\geq$ 99.5%) and all other reagents and solvents were of analytical reagent grade and were

purchased from Merck (KGaA, Darmstadt, Germany). Deionized (DI) water was used for the preparation of aqueous solutions.

2.2. Material Characterization

The functional groups of the synthesized materials were identified using an Alpha Bruker compact Fourier-transform infrared (FTIR) spectrophotometer (Frankfurt am Main, Germany) at room temperature over the wavenumber range between 400 and 4000 cm^{-1}. A JSM-6390LA JEOL scanning electron microscope (SEM), which operated at an accelerating voltage of 20 kV, was applied to visualize the surface morphology of the synthesized materials; this SEM instrument was coupled with a JED-2300 energy-dispersive X-ray spectroscope (EDXRF) (Tokyo, Japan) unit for the elemental analyses. The metal ion content was determined using an Optima 2100 DV Perkin-Elmer Optical Emission Spectrometer (ICP-OES) (Waltham, MA, USA).

2.3. Methods

2.3.1. Synthesis of the Composite

The $ZnFe_2O_4$ composite was synthesized by the co-precipitation of urea and iron(III) chloride with a zinc salt ($ZnCl_2$ or $Zn(CH_3COO)_2{\cdot}2H_2O$)). First, 6 mmol of urea, 1 mmol of a zinc salt ($ZnCl_2$ or $Zn(CH_3COO)_2{\cdot}2H_2O$)), and 1 mmol of $FeCl_3$ were all dissolved in a 100 mL water/methanol (1:1) mixed solvent. Then, the resultant mixed solution was stirred at 80 °C for 24 h, forming a colored precipitate. This precipitate was filtrated off with filter paper and washed with hot water. Finally, the purified product was heated in an electrical furnace for 3 h at 800 °C under ambient air. This thermal decomposition produced brown $ZnFe_2O_4$ composites, termed composite **1** when the zinc salt was $ZnCl_2$ and composite **2** when the zinc salt was $Zn(CH_3COO)_2{\cdot}2H_2O$. Composites **1** and **2** were grounded into powder and SEM/EDX and FTIR characterization were performed.

2.3.2. Synthesis of the Adsorbent Material

The $ZnFe_2O_4$-CNT adsorbent material was simply synthesized using the following steps: (i) mix 1.0 g of the fullerene CNT and 0.1 g of the $ZnFe_2O_4$ composite in a clean, dry porcelain mortar; (ii) combine the CNT material and the composite by grinding with a porcelain pestle for a few minutes; (iii) add a few drops of methanol solvent to the mixture and continue the grinding of the mixture thoroughly for ~20 min until the mixture is uniform; (iv) collect the resultant $ZnFe_2O_4$-CNT adsorbent material from the mortar and dry it in a vacuum desiccator containing anhydrous calcium chloride; (v) analyze the SEM/EDX and FTIR spectral data to structurally characterize the adsorbent material.

2.3.3. Heavy Metal Adsorption

Adsorption of the tested heavy metal ions (i.e., Hg(II), Pb(II), Cd(II) and Sn(II)) from aqueous solution using the synthesized adsorbent material was performed in batch mode. A 50 mL of standard aqueous metal ion solution (20 mg/100 mL) was put in a 50 mL glass bottle. Hydrochloric acid (0.01 N) or sodium hydroxide (0.01 N) was used to adjust the pH of the solution. Next, 50 mg of the synthesized adsorbent material was added to the solution, then the flask was shaken on a mechanical shaker at room temperature, after which 5 mL samples were taken by pipette from the solution after pre-defined time intervals and centrifuged for 10 min to remove the adsorbent. The concentration of non-adsorbed heavy metal ion left in the solution (C_e) was analyzed using an optical emission spectrometer. The removal efficiency was calculated as [33,34]:

$$\text{Removal efficiency (\%)} = (C_o - C_e)/C_o \times 100$$

where C_o is the initial concentration of the metal ion and C_e is the concentration of the metal ion at time *t*.

3. Results and Discussion

3.1. Composites 1 and 2

The co-precipitation of urea and $FeCl_3$ with $ZnCl_2$ (or $Zn(CH_3COO)_2{\cdot}2H_2O$) was attempted under the following reaction conditions: starting reagent, liquid–liquid interaction; stoichiometry, 6:1:1 (urea:$FeCl_3$:$ZnCl_2$); solvent, water/methanol (1:1); time, ~24 h; temperature, 80 °C.

The co-precipitation of these reagents under these reaction conditions yielded a brown $(Fe(NH_2CONH_2)_6)Cl_3$ and $(Zn(NH_2CONH_2)_6)Cl_2$ solid mixture, as described by the following Equations:

$$FeCl_3 + 6NH_2CONH_2 \overset{80\ ^\circ C}{\rightarrow} [Fe(NH_2CONH_2)_6]Cl_3 \quad (1)$$

$$ZnCl_2 + 6NH_2CONH_2 \overset{80\ ^\circ C}{\rightarrow} [Zn(NH_2CONH_2)_6]Cl_2 \quad (2)$$

Using $Zn(CH_3COO)_2{\cdot}2H_2O$ instead of $ZnCl_2$ also yielded a brown $(Fe(NH_2CONH_2)_6)Cl_3$ and $(Zn(NH_2CONH_2)_6)(CH_3COO)_2$ solid mixture, as described using the following Equations:

$$FeCl_3 + 6NH_2CONH_2 \overset{80\ ^\circ C}{\rightarrow} [Fe(NH_2CONH_2)_6]Cl_3 \quad (3)$$

$$Zn(CH_3COO)_2{\cdot}2H_2O + 6NH_2CONH_2 \overset{80\ ^\circ C}{\rightarrow} [Zn(NH_2CONH_2)_6](CH_3COO)_2 + 2H_2O \quad (4)$$

The IR spectra of the $(Fe(NH_2CONH_2)_6)Cl_3$ and $(Zn(NH_2CONH_2)_6)Cl_2$ and $(Fe(NH_2CONH_2)_6)Cl_3$ and $(Zn(NH_2CONH_2)_6)(CH_3COO)_2$ solid mixtures are presented in Figure 1. In general, both solid mixtures have similar IR profiles. The vibrational modes of the $(-NH_2)$ bonds of $\delta_{rock}(NH_2)$, $\delta_{twist}(NH_2)$, $\delta_{def}(NH_2)$, and $\nu(NH_2)$ were resonated at 620–533, 829–825, 1400–1396, and 3452–3372 cm^{-1}, respectively. Among these modes that originated from the $\nu(NH_2)$, vibrations appeared as broad, medium-strong intensity bands. The band resulting from the $\nu(C{=}O)$ vibrations was located at 1560–1558 cm^{-1}. The SEM images and EDX spectrum of $(Fe(NH_2CONH_2)_6)Cl_3$ and $(Zn(NH_2CONH_2)_6)Cl_2$ and $(Fe(NH_2CONH_2)_6)Cl_3$ and $(Zn(NH_2CONH_2)_6)(CH_3COO)_2$ solid mixtures are illustrated in Figure 2. Iron, zinc, carbon, oxygen, nitrogen, and chlorine elements are excited in both solid mixtures, as evidenced from their EDX spectra. Morphologically, there are differences in the microstructure, shape, and surface topology between both solid mixtures, as evidenced by their SEM images. The $(Fe(NH_2CONH_2)_6)Cl_3$ and $(Zn(NH_2CONH_2)_6)Cl_2$ solid mixture had mixtures of cotton-like and cloud-like particles. The $Fe(NH_2CONH_2)_6)Cl_3$ and $(Zn(NH_2CONH_2)_6)(CH_3COO)_2$ solid mixture had a stone-like morphology. These stones had different shapes and sizes. The SEM analysis indicated that the type of zinc salt ($ZnCl_2$ or $Zn(CH_3COO)_2{\cdot}2H_2O$) affects the morphology of the final solid mixture. Changing the zinc salt from chloride to acetate changed the morphology of the final solid mixture from an undefined structure (cotton- or cloud-shaped) to a more defined structure (stone-shaped).

Calcination of the $(Fe(NH_2CONH_2)_6)Cl_3$ and $(Zn(NH_2CONH_2)_6)Cl_2$ solid mixture in an electrical furnace for 3 h at 800 °C under the ambient air condition generated the reddish-brown-colored composite **1** (Zinc ferrite; $ZnFe_2O_4$), as described by the following equations:

$$2[Fe(NH_2CONH_2)_6]Cl_3 \overset{800\ ^\circ C}{\rightarrow} Fe_2O_3 + 7N_2 + 4NH_3 + 3CH_4 + 9CO + 6NH_4Cl \quad (5)$$

$$[Zn(NH_2CONH_2)_6]Cl_2 \overset{800\ ^\circ C}{\rightarrow} ZnO + 3N_2 + 4NH_3 + CH_4 + 5CO + 2NH_4Cl \quad (6)$$

$$Fe_2O_3 + ZnO \overset{800\ ^\circ C}{\rightarrow} ZnFe_2O_4(\text{Zinc ferrite}) \quad (7)$$

Calcination of the $(Fe(NH_2CONH_2)_6)Cl_3$ and $(Zn(NH_2CONH_2)_6)(CH_3COO)_2$ solid mixture in the same conditions generated the reddish-brown-colored composite **2** (zinc ferrite; $ZnFe_2O_4$) as described by the following equations:

$$2[Fe(NH_2CONH_2)_6]Cl_3 \overset{800\ ^\circ C}{\rightarrow} Fe_2O_3 + 7N_2 + 4NH_3 + 3CH_4 + 9CO + 6NH_4Cl \quad (8)$$

$$[Zn(NH_2CONH_2)_6](CH_3COO)_2 \overset{800\ ^\circ C}{\rightarrow} ZnO + 3N_2 + 4NH_3 + CH_4 + 5CO + 2CH_3COONH_4 \quad (9)$$

$$Fe_2O_3 + ZnO \overset{800\ ^\circ C}{\rightarrow} ZnFe_2O_4(\text{Zinc ferrite}) \quad (10)$$

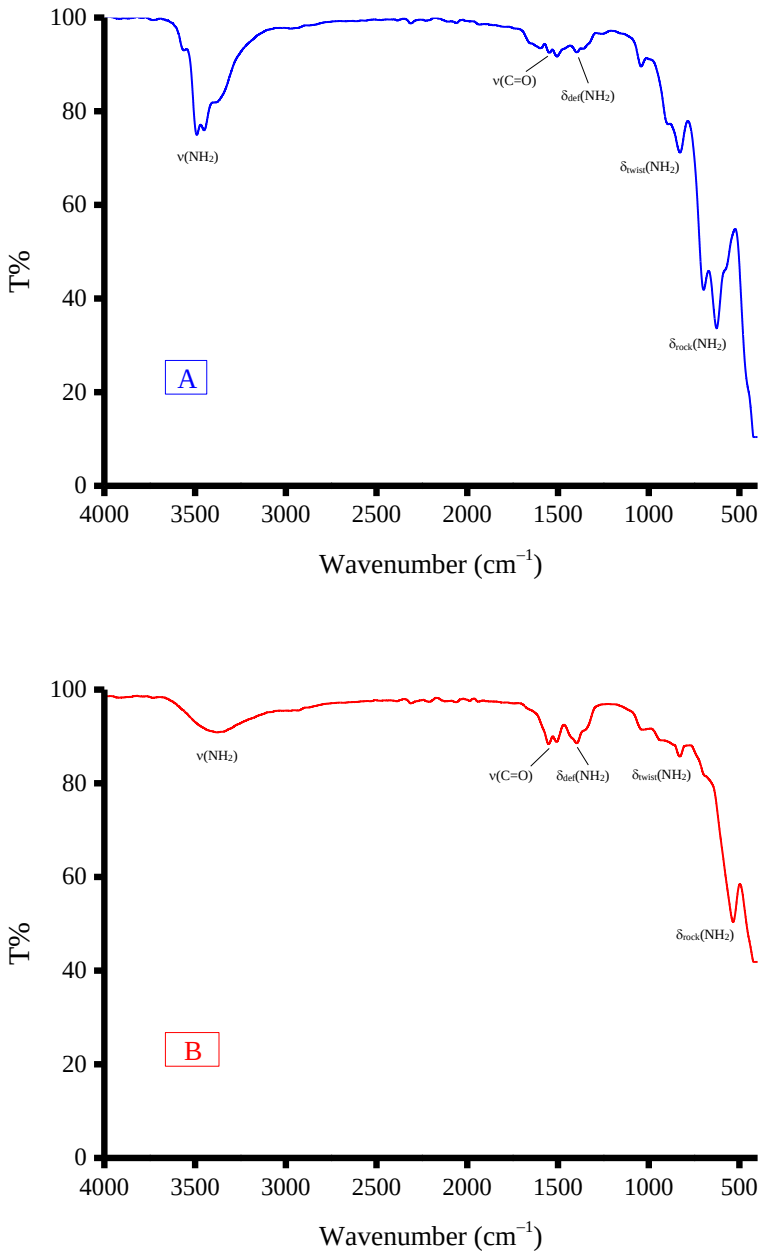

Figure 1. IR spectra of solid mixtures: (**A**) $(Zn(NH_2CONH_2)_6)Cl_2$ and $(Fe(NH_2CONH_2)_6)Cl_3$; (**B**) $(Zn(NH_2CONH_2)_6)(CH_3COO)_2$ and $(Fe(NH_2CONH_2)_6)Cl_3$.

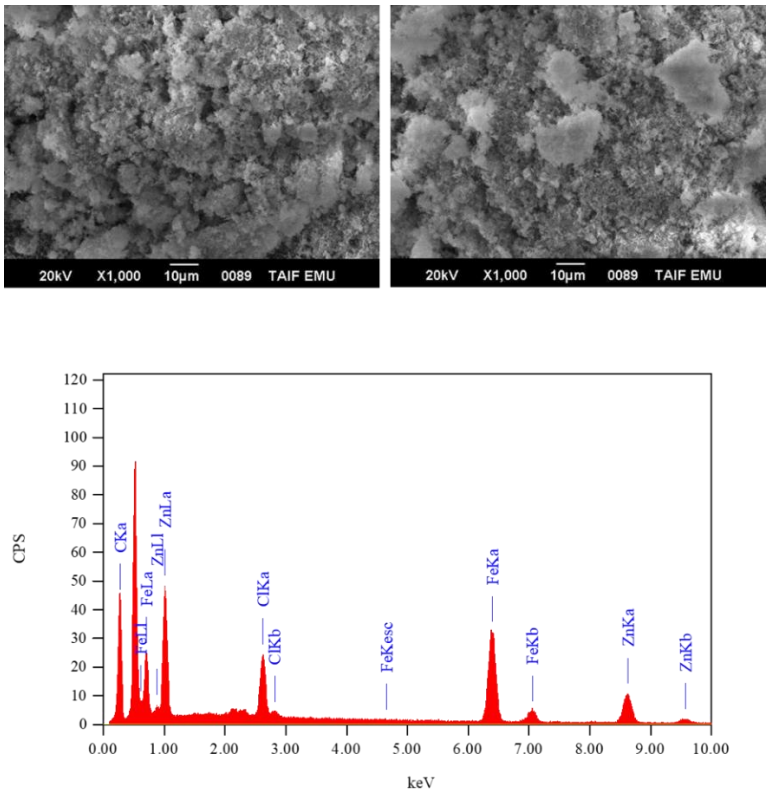

(**A**)

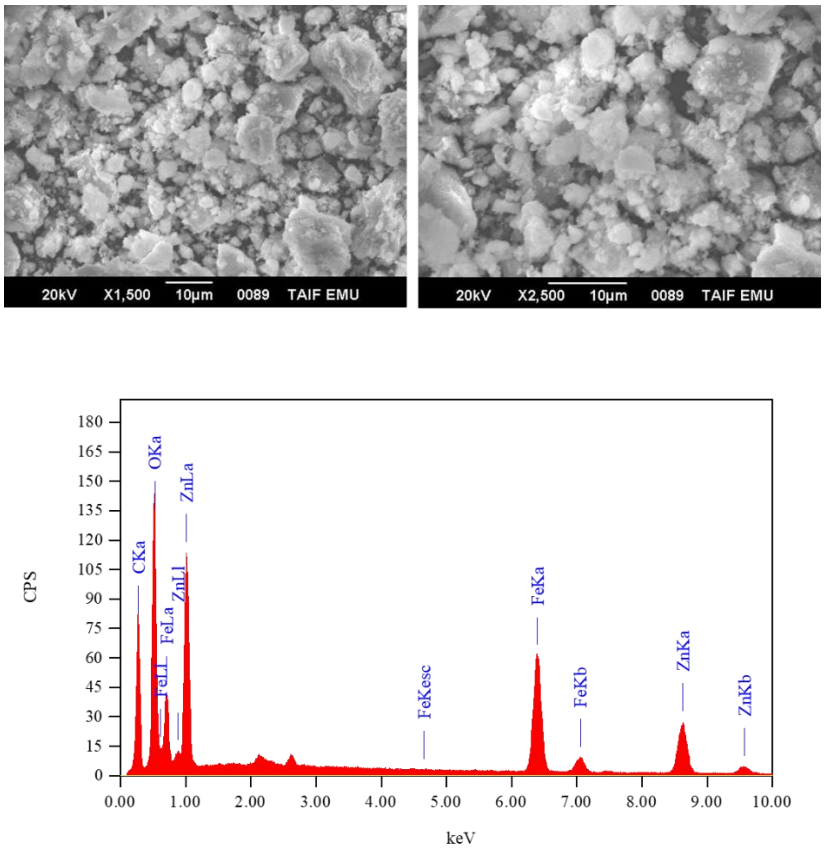

(**B**)

Figure 2. (**A**) SEM images and EDX spectra of solid mixtures: $(Zn(NH_2CONH_2)_6)Cl_2$ and $(Fe(NH_2CONH_2)_6)Cl_3$; (**B**) $Zn(NH_2CONH_2)_6)(CH_3COO)_2$ and $(Fe(NH_2CONH_2)_6)Cl_3$.

The IR spectra of composites **1** and **2** are presented in Figure 3. In general, both composites have similar IR features. The absorption bands that originated from the $\delta_{rock}(NH_2)$, $\delta_{twist}(NH_2)$, $\delta_{def}(NH_2)$, $\nu(NH_2)$, and $\nu(C=O)$ vibrations of the $-NH_2$ and C=O bonds in the solid mixtures were no longer observed in their corresponding composites. The IR spectra of composites **1** and **2** displayed only two absorption bands at 425 and 528 cm^{-1}, which originated from the ν(Zn–O) and ν(Fe–O) vibrations. The IR profiles of composites **1** and **2** support the chemical structures of these composites derived through the above equations ($ZnFe_2O_4$). The SEM images and EDX spectrum of composites **1** and **2** are illustrated in Figure 4. Calcination of the $(Fe(NH_2CONH_2)_6)Cl_3$ and $(Zn(NH_2CONH_2)_6)Cl_2$ solid mixture at 800 °C resulted in the formation of composite **1** ($ZnFe_2O_4$), with changes in the morphology from a mixed cotton-like and cloud-like structure to a grass-like structure. In contrast, burning of the $(Fe(NH_2CONH_2)_6)Cl_3$ and $(Zn(NH_2CONH_2)_6)(CH_3COO)_2$ solid mixture at 800 °C resulted in the formation of composite **2** ($ZnFe_2O_4$), with changes in the morphology from a stone-like structure to a coral-reef-like structure. The EDX spectra evidenced the presence of iron, zinc, and oxygen elements in both composites, with mass percentages of 46.30%, 27.58% and 26.50% for composite **1**, respectively; and of 46.61%, 27.08% and 26.69% for composite **2**, respectively. These elemental compositions agree well with the proposed chemical structures for composites **1** and **2** ($ZnFe_2O_4$). Around 4% of the carbon element was also found in the EDX spectra of composites **1** and **2**, which indicated that some carbons remained as residuals from the calcination of solid mixtures at 800 °C.

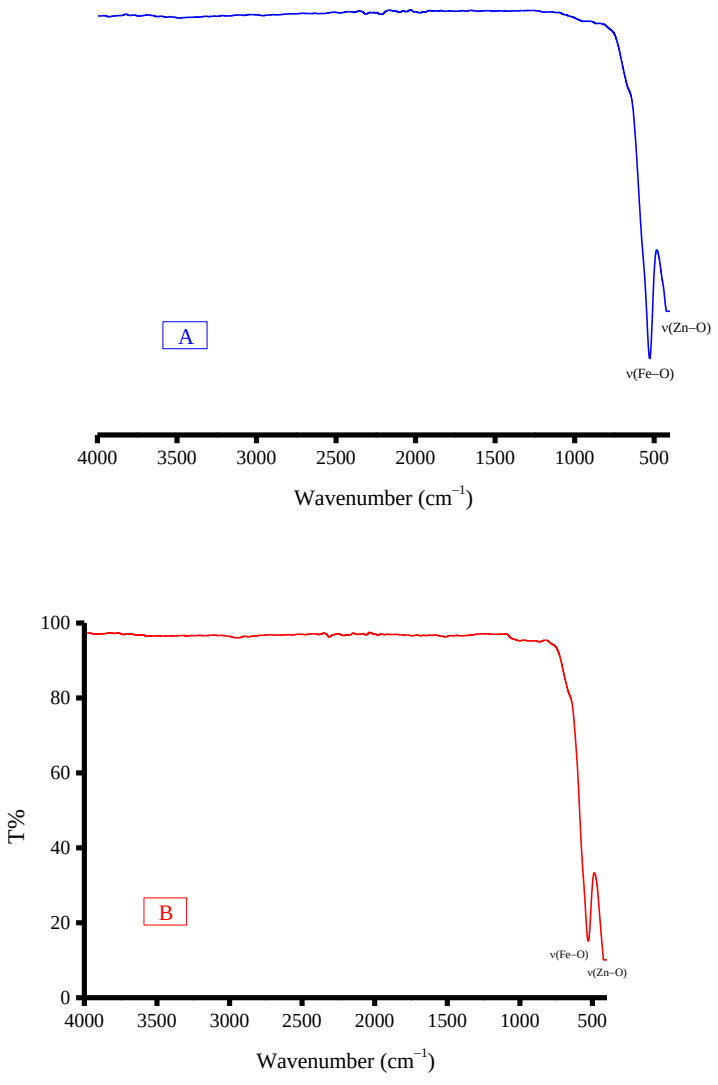

Figure 3. IR spectra of the composites: (**A**) composite **1**; (**B**) composite **2**.

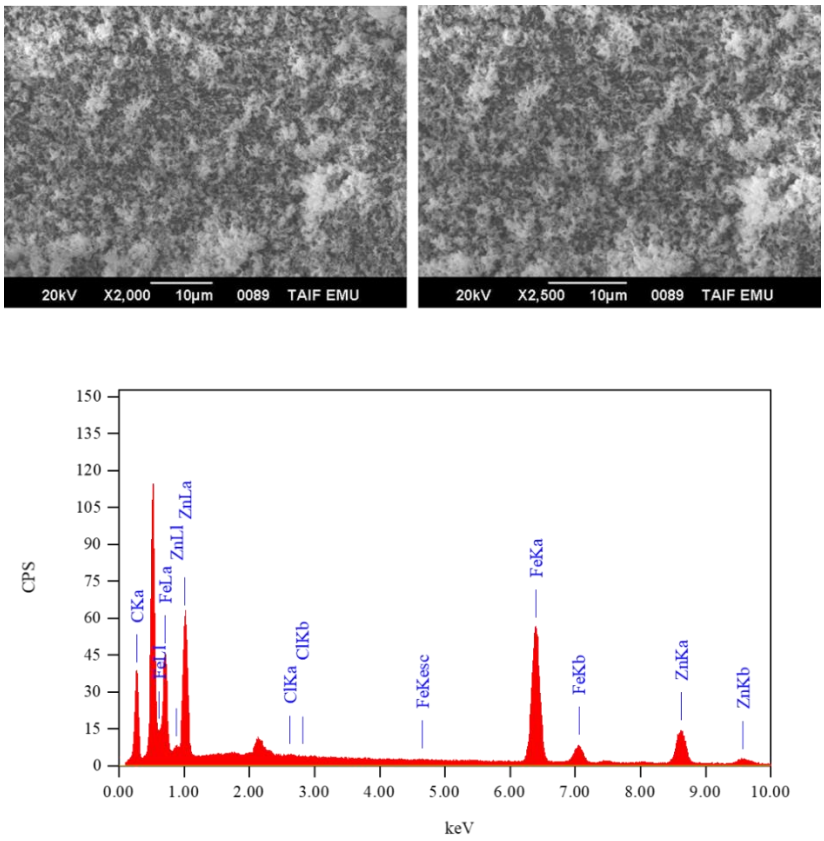

Figure 4. SEM images and EDX spectra of the composites: (**A**) composite **1**; (**B**) composite **2**.

3.2. $ZnFe_2O_4$-CNT Adsorbent

Multiwalled fullerene carbon nanotubes (CNTs) were used as the carbon material for the synthesis of the $ZnFe_2O_4$-CNT adsorbent material. Figure 5 shows the IR spectrum of the fullerene carbon nanotube (CNT), while its SEM/EDX results are given in Figure 6. In the IR spectrum of fullerene CNT, no clear IR absorption bands were observed across the wavenumber range of 4000 to 400 cm^{-1}. The EDX spectrum of fullerene CNT showed that this material is 100% pure carbon, while the SEM images of this material captured at different magnifications (i.e., 3000, 5000, 7000 and 10,000×) visualized the nanotubes. The crushing of the fullerene CNT material with the synthesized $ZnFe_2O_4$ composite material was attempted under the following reaction conditions: starting reagent, solid–solid interaction; stoichiometry, 10:1 (CNT to composite); solvent, several drops of methanol solvent; time, ~20 min; temperature, ambient.

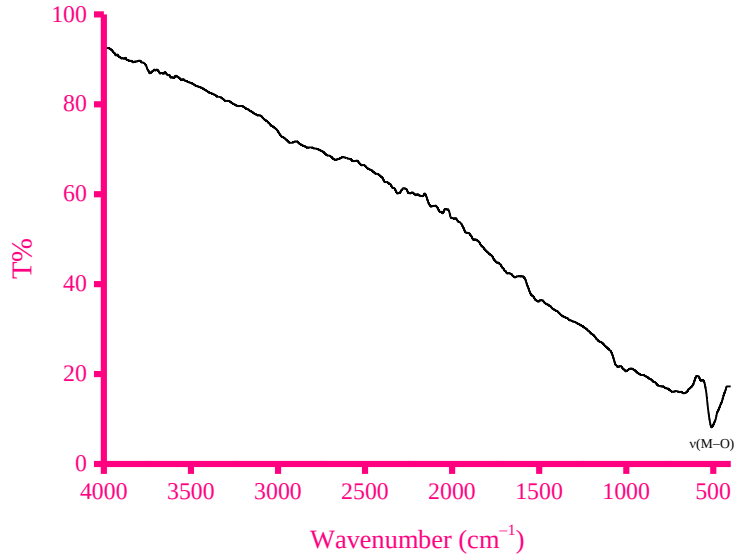

Figure 5. IR spectrum of the fullerene carbon nanotube (CNT).

The crushing of these materials under these reaction conditions yielded a homogenate solid black-colored $ZnFe_2O_4$-CNT adsorbent. Figure 7 illustrates the magnetic property of the synthesized $ZnFe_2O_4$-CNT adsorbent material. The IR spectrum of the synthesized adsorbent material is given in Figure 8, while its surface morphology along with the EDX profile is given in Figure 9. In the IR spectrum of the $ZnFe_2O_4$-CNT adsorbent, only one clear IR band was observed at 508 cm^{-1}, which was assigned to the ν(M–O) vibrations (M: Zn or Fe). SEM/EDX analysis was conducted to collect information regarding the elemental composition, surface topology, shape, and size of the synthesized $ZnFe_2O_4$-CNT adsorbent material. Iron, zinc, carbon, and oxygen elements were present in the adsorbent material, as evidenced from its EDX profile. The SEM images of the adsorbent material revealed that it consisted of large aggregates, while several particles with different irregular features, sizes, and shapes were accumulated over these aggregates.

3.3. Adsorption of Heavy Metal Ions

Adsorption of four heavy metal ions (i.e., Hg(II), Pb(II), Cd(II), and Sn(II)) over the synthesized $ZnFe_2O_4$-CNT adsorbent material was investigated and compared with that of the fullerene CNT material under the following conditions: adsorbent content, 10–50 mg; metal ion concentration, 20 mg/100 mL; pH, 2–8; time, 5–20 min; temperature, ambient.

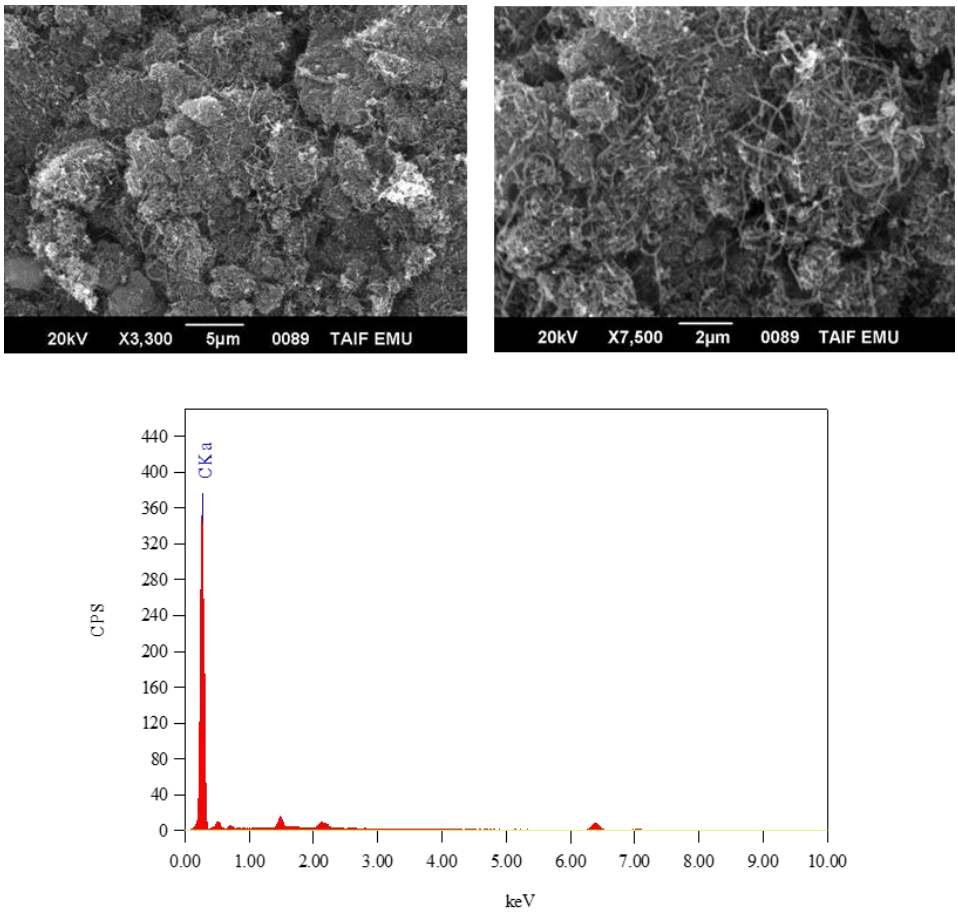

Figure 6. SEM images and EDX spectrum of the fullerene carbon nanotube (CNT).

Figure 7. The magnetic properties of the $ZnFe_2O_4$-CNT adsorbent.

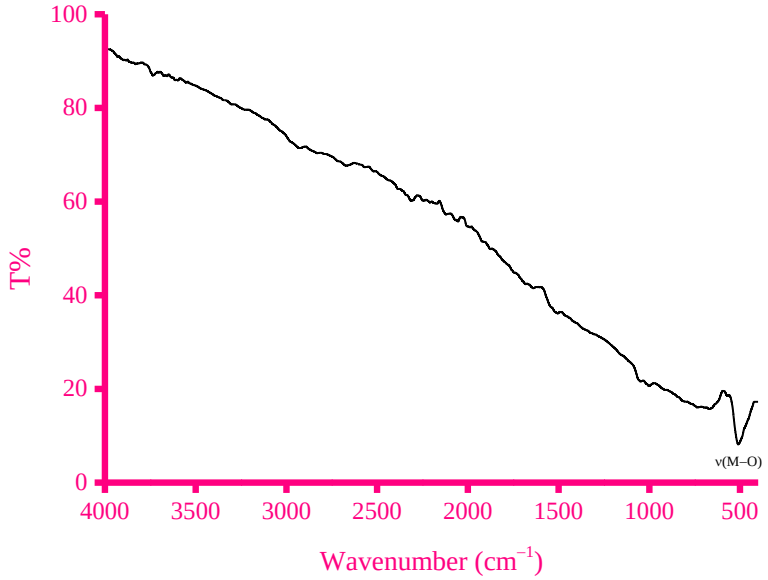

Figure 8. IR spectrum of the $ZnFe_2O_4$-CNT adsorbent.

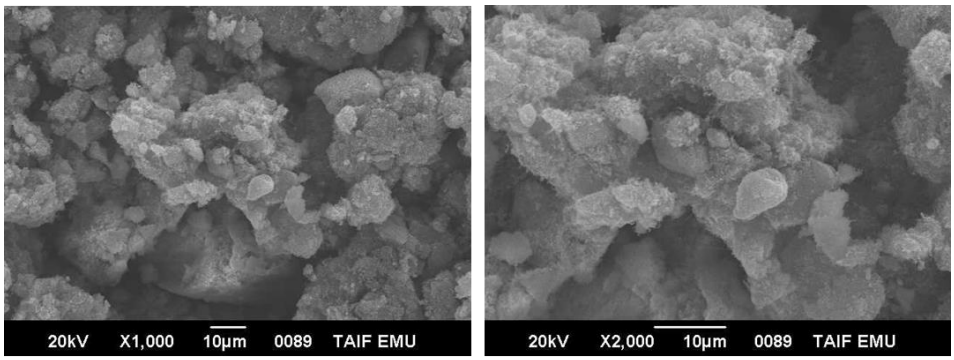

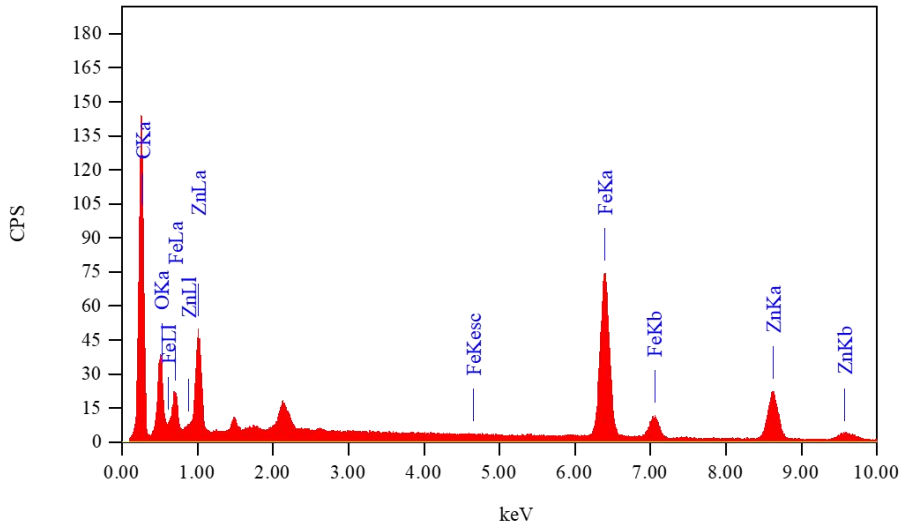

Figure 9. SEM micrographs and EDX spectrum of the $ZnFe_2O_4$-CNT adsorbent.

3.3.1. Effects of the pH

The effects of the pH on the removal of the investigated heavy metal ions (Hg(II), Pb(II), Cd(II) and Sn(II)) by the synthesized $ZnFe_2O_4$-CNT adsorbent material was examined

within the pH range of 2–8. Hydrochloric acid (0.01 N) or sodium hydroxide (0.01 N) was used to adjust the pH of the solution. Fifty milligrams of the synthesized $ZnFe_2O_4$-CNT adsorbent material was added to a 50 mL aqueous solution containing metal ion (20 mg/100 mL), then the mixture was mechanically shaken at room temperature. Sample aliquots of 5 mL were taken every 5 min, centrifuged for 10 min to remove the adsorbent material, and the concentration of non-adsorbed metal ion remaining in the solution was determined using an optical emission spectrometer to calculate the removal efficiency (%). Figure 10 presents the removal efficiency (%) of heavy metal ions using 50 mg of $ZnFe_2O_4$-CNT adsorbent at different pH values. This figure indicates that the maximum removal of the Hg(II) and Pb(II) ions occurred at pH = 5.0, while the maximum removal of the Cd(II) and Sn(II) ions occurred at pH = 6.0.

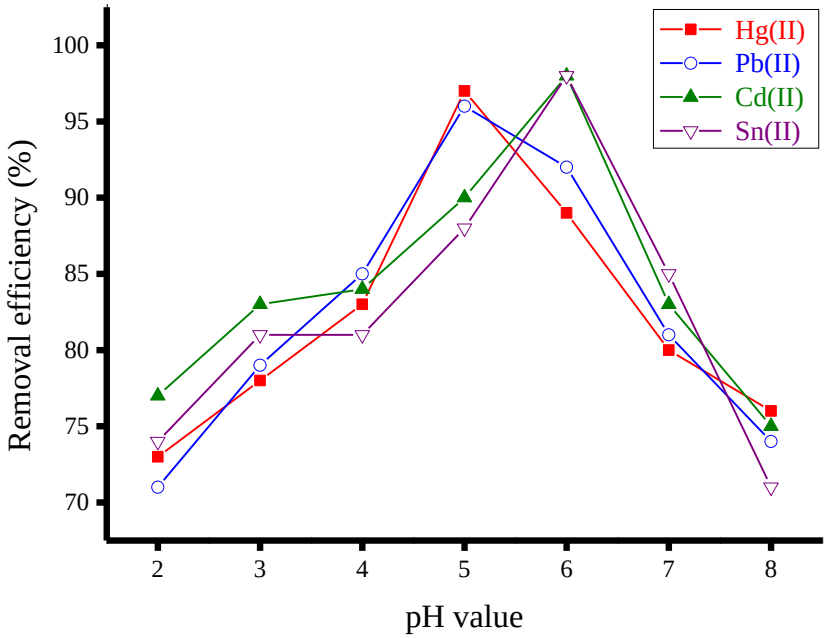

Figure 10. Removal efficiency (%) of heavy metal ions (20 mg/100 mL) using 50 mg of the synthesized $ZnFe_2O_4$-CNT adsorbent material at different pH values.

3.3.2. Effects of the Adsorbent Dosage

The effects of the adsorbent dosage on the removal of the investigated heavy metal ions (Hg(II), Pb(II), Cd(II) and Sn(II)) by the synthesized $ZnFe_2O_4$-CNT adsorbent material were examined using varying amounts of adsorbent (10–50 mg). Figure 11 presents the removal efficiency (%) of heavy metal ions (20 mg/100 mL) using different amounts of $ZnFe_2O_4$-CNT adsorbent. This figure indicates that the removal efficiency (%) of heavy metal ions increased with the increase of the amount of the adsorbent until 50 mg; after this value, the removal efficiency was constant. This indicates that the appropriate dosage for the $ZnFe_2O_4$-CNT adsorbent for removal of each of the heavy metal ions from aqueous solution at a concentration of 20 mg/100 mL is 50 mg.

3.3.3. Effects of the Contact Time

The effects of the contact time on the removal of the investigated heavy metal ions (Hg(II), Pb(II), Cd(II), and Sn(II)) by the synthesized $ZnFe_2O_4$-CNT adsorbent material were examined at different contact times (5–25 min) while keeping other factors constant (adsorbent dosage is 50 mg, pH = 5 for the Hg(II) and Pb(II) ions, pH = 6 for the Cd(II) and Sn(II) ions). Figure 12 illustrates the removal efficiency (%) of heavy metal ions (20 mg/100 mL) using 50 mg of synthesized $ZnFe_2O_4$-CNT adsorbent material. The outcomes from this figure indicated that 97–99% of the investigated heavy metal content was adsorbed by the $ZnFe_2O_4$-CNT adsorbent in 15 min. The test was repeated using

50 mg of the free fullerene CNT material, which showed that it adsorbed around 97–99% of the heavy metal content within 20 min (Figure 13), indicating that crushing fullerene CNT with $ZnFe_2O_4$ composite improves the adsorption property of free fullerene CNT towards heavy metal ions (i.e., Hg(II), Pb(II), Cd(II), and Sn(II)) by 25%.

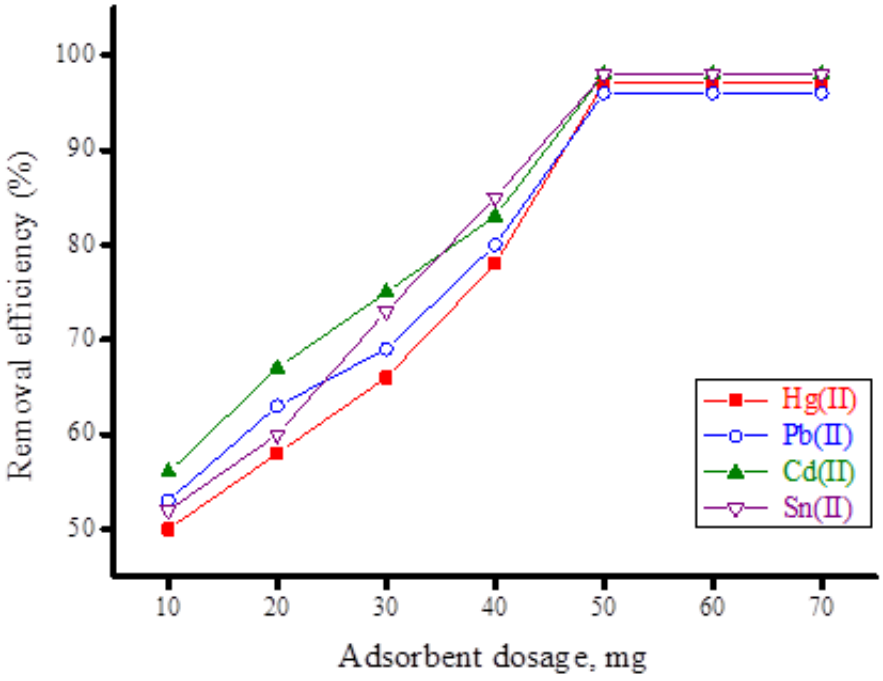

Figure 11. Removal efficiency (%) of heavy metal ions (20 mg/100 mL) using different amounts of synthesized ZnF_2O_4-CNT adsorbent material.

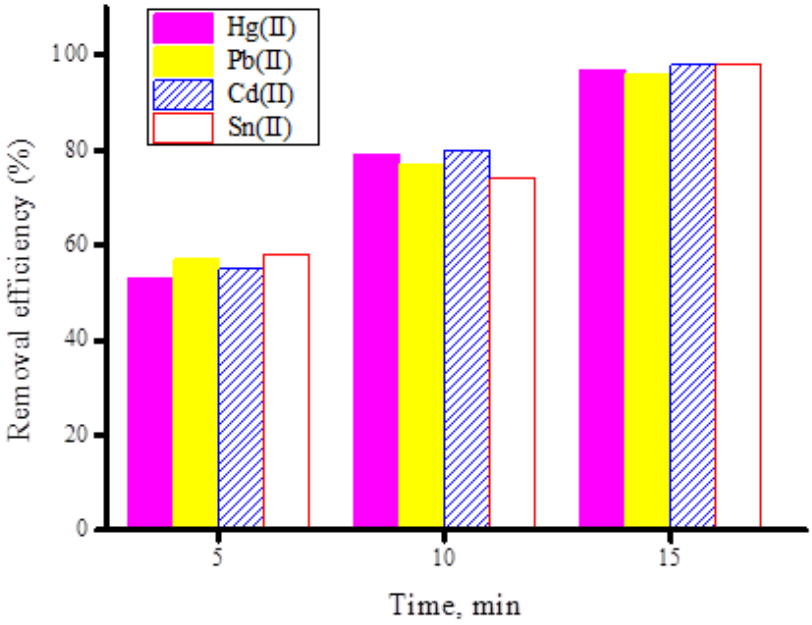

Figure 12. Removal efficiency (%) of heavy metal ions (20 mg/100 mL) using 50 mg of the synthesized $ZnFe_2O_4$-CNT adsorbent material at different contact times.

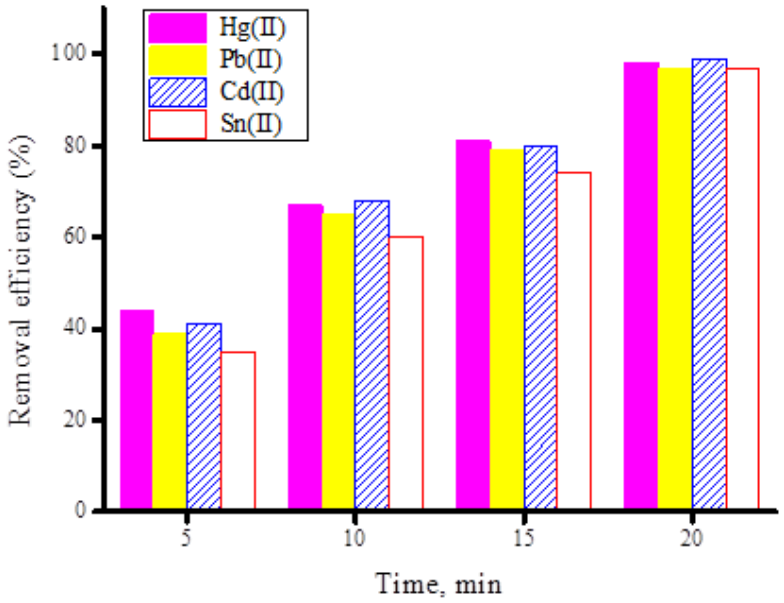

Figure 13. Removal efficiency (%) of heavy metal ions (20 mg/100 mL) using 50 mg of free fullerene CNT material at different contact times.

3.4. Adsorption Mechanisms, Regeneration and Reusability

Fullerenes have high electron affinity, a high surface-to-volume ratio, and surface defects. Fullerene CNTs can adsorb the heavy metal ions (Hg(II), Pb(II), Cd(II), and Sn(II)) into the defects or spaces between the carbon nanoclusters via pore diffusion, intra-particle diffusion, film diffusion, or surface complexation formation [2,24,35]. The mesoporous spaces of carbon nanoclusters can be occupied by the heavy metal ions (physisorption) during the adsorption process. Crushing fullerene CNT with the $ZnFe_2O_4$ composite improves the adsorption performance of free fullerene CNT towards the investigated heavy metal ions by 25%, probably due to the physicochemical bond between the heavy metal ions and the $ZnFe_2O_4$ composite. The reusability of $ZnFe_2O_4$-CNT adsorbent was performed by studding the desorption efficiency of the adsorbent material under the following conditions: adsorbent dosage, 50 mg; metal ion concentration, 20 mg/100 mL; pH = 5 for the Hg(II) and Pb(II) ions, pH = 6 for the Cd(II) and Sn(II) ions; contact time, 15 min; temperature, ambient. After the adsorption experiment, the $ZnFe_2O_4$-CNT adsorbent was removed from the solution by filtration and washed with deionized water. Six different desorbing chemicals were examined (0.1 N EDTA, 0.1 N KOH, 0.1 N HNO_3, 0.1 N HCl, 0.1 N H_2SO_4, and deionized water) to remove the adsorbed heavy metal ion from the $ZnFe_2O_4$-CNT adsorbent. It was found that EDTA (~83%) and HNO_3 (~92.5%) were the most efficient eluting agents for recovery of the investigated heavy metal ions from the adsorbent. An adsorption–desorption experiment was run for several cycles to determine the reusability of the $ZnFe_2O_4$-CNT adsorbent, showing that the adsorbent can be reused at least ten times in adsorption–desorption cycles.

4. Conclusions

As a result of the rapid global population growth and development of society, water purification processes have become important major challenges for researchers in wastewater management. Human societies release large quantities of wastewater containing toxic organic and inorganic compounds, such as organic pollutants and heavy metal ions, which have become a combined threat to aquatic environments, plants, animals, and human health; therefore, it is necessary to reused wastewater from these pollutants through suitable treatment processes or to remove these pollutants before the wastewater is discharged into the environment. In this study, our purpose was to increase the adsorption property

of fullerene carbon nanotubes (CNT) towards hazardous heavy metals by combining the CNT with a $ZnFe_2O_4$ composite. The combination of the two materials was accomplished via a grinding process that yielded a black homogenate solid $ZnFe_2O_4$-CNT adsorbent material. The synthesized adsorbent material was physicochemically characterized and its adsorption performance towards four heavy metal ions (i.e., Hg(II), Pb(II), Cd(II), and Sn(II)) was examined. The optimum conditions to effectively recover the investigated metal ions at a concentration of 20 mg/100 mL from aqueous solution are: pH = 5 for the Hg(II) and Pb(II) ions and pH = 6 for the Cd(II) and Sn(II) ions, contact time = 15 min, and adsorbent dosage = 50 mg. Crushing fullerene CNTs with $ZnFe_2O_4$ composite improves the adsorption performance of free fullerene CNTs towards the investigated heavy metal ions by 25%.

Author Contributions: Conceptualization, A.M.A. and T.A.A.; data curation, H.A.S. and M.S.R.; formal analysis, H.A.S., M.A. and M.S.H.; funding acquisition, A.M.A.; investigation, M.A. and M.S.H.; methodology, M.S.H.; project administration, A.M.A.; resources, A.A.A. and M.S.R.; software, H.A.S., A.A.A. and M.S.R.; validation, A.A.A.; visualization, M.A. and T.A.A.; writing—original draft, M.A.; writing—review and editing, A.M.A. All authors have read and agreed to the published version of the manuscript.

Funding: This work was funded by the Deputyship for Research and Innovation, Ministry of Education, Saudi Arabia; project number: 124-441-1.

Institutional Review Board Statement: Not applicable.

Informed Consent Statement: Not applicable.

Data Availability Statement: Not applicable.

Acknowledgments: The authors extend their appreciation to the Deputyship for Research and Innovation, Ministry of Education, Saudi Arabia, for funding this research work through project number 124-441-1.

Conflicts of Interest: The authors declare no conflict of interest.

References

1. Tariq, M.; Muhammad, M.; Khan, J.; Raziq, A.; Uddin, M.K.; Niaz, A.; Ahmed, S.S.; Rahim, A. Removal of Rhodamine B dye from aqueous solutions using photo-Fenton processes and novel Ni–Cu@MWCNTs photocatalyst. *J. Mol. Liq.* **2020**, *312*, 113399. [CrossRef]
2. Baby, R.; Saifullah, B.; Hussein, M.Z. Carbon Nanomaterials for the Treatment of Heavy Metal-Contaminated Water and Environmental Remediation. *Nanoscale Res. Lett.* **2019**, *14*, 1–17. [CrossRef]
3. Sharma, M.; Poddar, M.; Gupta, Y.; Nigam, S.; Avasthi, D.; Adelung, R.; Abolhassani, R.; Fiutowski, J.; Joshi, M.; Mishra, Y. Solar light assisted degradation of dyes and adsorption of heavy metal ions from water by CuO–ZnO tetrapodal hybrid nanocomposite. *Mater. Today Chem.* **2020**, *17*, 100336. [CrossRef]
4. Lv, W.; Zhao, K.; Ma, S.; Kong, L.; Dang, Z.; Chen, J.; Zhang, Y.; Hu, J. Process of removing heavy metal ions and solids suspended in micro-scale intensified by hydrocyclone. *J. Clean. Prod.* **2020**, *263*, 121533. [CrossRef]
5. Kumar, V.; Thakur, R.K.; Kumar, P. Assessment of heavy metals uptake by cauliflower (*Brassica oleracea* var. botrytis) grown in integrated industrial effluent irrigated soils: A prediction modeling study. *Sci. Hortic.* **2019**, *257*, 108682. [CrossRef]
6. Kumar, S.; Prasad, S.; Yadav, K.K.; Shrivastava, M.; Gupta, N.; Nagar, S.; Bach, Q.-V.; Kamyab, H.; Khan, S.A.; Yadav, S.; et al. Hazardous heavy metals contamination of vegetables and food chain: Role of sustainable remediation approaches—A review. *Environ. Res.* **2019**, *179*, 108792. [CrossRef]
7. Hasanpour, M.; Hatami, M. Photocatalytic performance of aerogels for organic dyes removal from wastewaters: Review study. *J. Mol. Liq.* **2020**, *309*, 113094. [CrossRef]
8. Chi, Y.; Chen, Y.; Hu, C.; Wang, Y.; Liu, C. Preparation of Mg–Al–Ce triple-metal composites for fluoride removal from aqueous solutions. *J. Mol. Liq.* **2017**, *242*, 416–422. [CrossRef]
9. Peng, W.; Li, H.; Liu, Y.; Song, S. A review on heavy metal ions adsorption from water by graphene oxide and its composites. *J. Mol. Liq.* **2017**, *230*, 496–504. [CrossRef]
10. Guo, T.; Bulin, C.; Li, B.; Zhao, Z.; Yu, H.; Sun, H.; Ge, X.; Xing, R.; Zhang, B. Efficient removal of aqueous Pb(II) using partially reduced graphene oxide-Fe_3O_4. *Adsorpt. Sci. Technol.* **2018**, *36*, 1031–1048. [CrossRef]
11. Lei, X.; Li, X.; Ruan, Z.; Zhang, T.; Pan, F.; Li, Q.; Xia, D.; Fu, J. Adsorption-photocatalytic degradation of dye pollutant in water by graphite oxide grafted titanate nanotubes. *J. Mol. Liq.* **2018**, *266*, 122–131. [CrossRef]

12. Zeng, Q.-F.; Fu, J.; Zhou, Y.; Shi, Y.-T.; Zhu, H.-L. Photooxidation Degradation of Reactive Brilliant Red K-2BP in Aqueous Solution by Ultraviolet Radiation/Sodium Hypochlorite. *CLEAN Soil Air Water* **2009**, *37*, 574–580. [CrossRef]
13. Ahmadipouya, S.; Haris, M.H.; Ahmadijokani, F.; Jarahiyan, A.; Molavi, H.; Moghaddam, F.M.; Rezakazemi, M.; Arjmand, M. Magnetic Fe_3O_4@UiO-66 nanocomposite for rapid adsorption of organic dyes from aqueous solution. *J. Mol. Liq.* **2021**, *322*, 114910. [CrossRef]
14. Kumar, S.; Kaushik, R.D.; Purohit, L.P. Novel ZnO tetrapod-reduced graphene oxide nanocomposites for enhanced photocatalytic degradation of phenolic compounds and MB dye. *J. Mol. Liq.* **2021**, *327*, 114814. [CrossRef]
15. Baziar, M.; Zakeri, H.R.; Askari, S.G.; Nejad, Z.D.; Shams, M.; Anastopoulos, I.; Giannakoudakis, D.A.; Lima, E.C. Metal-organic and Zeolitic imidazole frameworks as cationic dye adsorbents: Physicochemical optimizations by parametric modeling and kinetic studies. *J. Mol. Liq.* **2021**, *332*, 115832. [CrossRef]
16. Bazzarella, A.Z.; Paquini, L.D.; Favero, U.G.; Alves, R.D.O.; Altoé, M.A.S.; Profeti, D.; Profeti, L.P.R. Cu-bentonite as a low-cost adsorbent for removal of ethylenethiourea from aqueous solutions. *J. Mol. Liq.* **2021**, *333*, 115912. [CrossRef]
17. Ibrahim, A.O.; Adegoke, K.A.; Adegoke, R.O.; AbdulWahab, Y.A.; Oyelami, V.B.; Adesina, M.O. Adsorptive removal of different pollutants using metal-organic framework adsorbents. *J. Mol. Liq.* **2021**, *333*, 115593. [CrossRef]
18. Fu, Y.; Yang, C.; Zheng, Y.; Jiang, J.; Sun, Y.; Chen, F.; Hu, J. Sulfur crosslinked poly(m-aminothiophenol)/potato starch on mesoporous silica for efficient Hg(II) removal and reutilization of waste adsorbent as a catalyst. *J. Mol. Liq.* **2021**, *328*, 115420. [CrossRef]
19. Dou, W.; Liu, J.; Li, M. Competitive adsorption of Cu^{2+} in Cu^{2+}, Co^{2+} and Ni^{2+} mixed multi–metal solution onto graphene oxide (GO)–based hybrid membranes. *J. Mol. Liq.* **2021**, *322*, 114516. [CrossRef]
20. Suresh, M.; Sivasamy, A. Fabrication of graphene nanosheets decorated by nitrogen-doped ZnO nanoparticles with enhanced visible photocatalytic activity for the degradation of Methylene Blue dye. *J. Mol. Liq.* **2020**, *317*, 114112. [CrossRef]
21. Chowdhury, M.F.; Khandaker, S.; Sarker, F.; Islam, A.; Rahman, M.T.; Awual, R. Current treatment technologies and mechanisms for removal of indigo carmine dyes from wastewater: A review. *J. Mol. Liq.* **2020**, *318*, 114061. [CrossRef]
22. López, S.L.F.; Virgen, M.R.M.; Montoya, V.H.; Morán, M.A.M.; Gómez, R.T.; Vázquez, N.A.R.; Cruz, M.A.P.; González, M.S.E. Effect of an external magnetic field applied in batch adsorption systems: Removal of dyes and heavy metals in binary solutions. *J. Mol. Liq.* **2018**, *269*, 450–460. [CrossRef]
23. Li, P.; Li, X.; Dai, S. Adsorption of gold in gold-thiosulfate solution onto a quartz surface. *J. Mol. Liq.* **2021**, *335*, 116114. [CrossRef]
24. Kroto, H.W.; Heath, J.R.; O'Brien, S.C.; Curl, R.F.; Smalley, R.E. C_{60}: Buckminsterfullerene. *Nature* **1985**, *318*, 162–163. [CrossRef]
25. Alekseeva, O.V.; Bagrovskaya, N.A.; Noskov, A.V. Sorption of heavy metal ions by fullerene and polystyrene/fullerene film compositions. *Prot. Met. Phys. Chem. Surf.* **2016**, *52*, 443–447. [CrossRef]
26. Yang, L.X.; Xu, Y.-B.; Jin, R.-C.; Wang, F.; Yin, P.; Li, G.-H.; Xu, C.-P.; Pan, L.-B. Nonstoichiometric M-ferrite porous spheres: Preparation, shape evolution and magnetic properties. *Ceram. Int.* **2015**, *41*, 2309–2317. [CrossRef]
27. Park, H.-S.; Koduru, J.R.; Choo, K.-H.; Lee, B. Activated carbons impregnated with iron oxide nanoparticles for enhanced removal of bisphenol A and natural organic matter. *J. Hazard. Mater.* **2015**, *286*, 315–324. [CrossRef]
28. Lingamdinne, L.P.; Koduru, J.R.; Karri, R.R. A comprehensive review of applications of magnetic graphene oxide based nanocomposites for sustainable water purification. *J. Environ. Manag.* **2019**, *231*, 622–634. [CrossRef]
29. Mishra, S.; Yadav, S.S.; Rawat, S.; Singh, J.; Koduru, J.R. Corn husk derived magnetized activated carbon for the removal of phenol and para-nitrophenol from aqueous solution: Interaction mechanism, insights on adsorbent characteristics, and isothermal, kinetic and thermodynamic properties. *J. Environ. Manag.* **2019**, *246*, 362–373. [CrossRef]
30. Sahoo, R.; Santra, S.; Ray, C.; Pal, A.; Negishi, Y.; Ray, S.K.; Pal, T. Hierarchical growth of $ZnFe_2O_4$ for sensing applications. *New J. Chem.* **2016**, *40*, 1861–1871. [CrossRef]
31. Lingamdinne, L.P.; Koduru, J.R.; Chang, Y.-Y.; Karri, R.R. Process optimization and adsorption modeling of Pb(II) on nickel ferrite-reduced graphene oxide nano-composite. *J. Mol. Liq.* **2018**, *250*, 202–211. [CrossRef]
32. Andjelković, L.; Šuljagić, M.; Lakić, M.; Jeremić, D.; Vulić, P.; Nikolić, A.S. A study of the structural and morphological properties of Ni–ferrite, Zn–ferrite and Ni–Zn–ferrites functionalized with starch. *Ceram. Int.* **2018**, *44*, 14163–14168. [CrossRef]
33. Dükkancı, M.; Gündüz, G.; Yılmaz, S.; Prihod'Ko, R. Heterogeneous Fenton-like degradation of Rhodamine 6G in water using CuFeZSM-5 zeolite catalyst prepared by hydrothermal synthesis. *J. Hazard. Mater.* **2010**, *181*, 343–350. [CrossRef] [PubMed]
34. Centi, G.; Perathoner, S.; Torre, T.; Verduna, M.G. Catalytic wet oxidation with H_2O_2 of carboxylic acids on homogeneous and heterogeneous Fenton-type catalysts. *Catal. Today* **2000**, *55*, 61–69. [CrossRef]
35. Kabir, M.M.; Mouna, S.S.P.; Akter, S.; Khandaker, S.; Alam, D.U.; Bahadur, N.M.; Mohinuzzaman, M.; Islam, A.; Shenashen, M. Tea waste based natural adsorbent for toxic pollutant removal from waste samples. *J. Mol. Liq.* **2021**, *322*, 115012. [CrossRef]